



Microstructure-based high-quality factor terahertz metamaterial bio-detection sensor

Zeng Qu^{1,2} · Jinfeng Kang^{1,3} · Wei Li^{1,3} · Boyi Yao^{1,3} · Hao Deng^{1,3} · Yiqing Wei^{1,3} · Huihui Jing^{1,3} · Xiaohong Li^{1,3} · Junping Duan^{1,3} · Binzhen Zhang^{1,3}

Received: 20 August 2022 / Revised: 15 April 2023 / Accepted: 23 April 2023 / Published online: 16 May 2023
© The Author(s), under exclusive licence to Springer Nature Switzerland AG 2023

Abstract

The sensitivity, accuracy, and stability of terahertz biodetection functional devices still need to be improved. A metamaterial-based terahertz biodetection sensor was to be designed and fabricated to meet this need. The sensor uses lithography and magnetron sputtering processes to prepare copper combination square ring microstructures. The sensor interacts with the incident terahertz wave to generate a magnetic dipole resonance, including a resonant peak with 98.9% absorption at the resonant frequency of 0.4696 THz. When the analyte's refractive index increased from 1.0 to 2.0, the resonance peak of the sensor obviously redshifted, and the absorption of the resonance peak almost exceeded 99%. Meanwhile, the sensitivity of the sensor can reach 78.6 GHz/RIU (refractive index unit, RIU), Q (quality factor) is up to 55.3, and FOM (figure of merit, FOM) is up to 9.81. In addition, the quadruple rotation structure makes the sensor insensitive to wide incidence angles and polarization. The designed sensor has excellent resonance characteristics and can realize the detection and identification of biomolecules with different refractive indices. It also provides new ideas for designing terahertz band bio-detection sensors and has critical applications in medical diagnosis and real-time monitoring.

Keywords Terahertz · High-Q · Metamaterial bio-detection sensors

1 Introduction

Bio-sensors are essential in disease diagnosis and prevention, food safety, and biomolecular research [1]. Labeling methods based on labeling sensors are widely used in gene and protein detection, including fluorescent labeling, enzyme labeling, and radionuclide labeling. However, that method requires pre-treatment of samples [2], significantly limiting the application scope and detection accuracy. It is

important to develop biosensors with high accuracy, sensitivity, stability, and labeling-free [3–5].

Metamaterials are a new material class that has emerged since the twenty-first century. It is a rationally designed composite material in which an array of microstructures designed artificially superimposed on a common material is made to exhibit extraordinary physical properties that natural materials do not possess [6–8]. For example, light and electromagnetic waves can change their usual properties, and such effects are impossible with conventional materials [9–11]. There is nothing special in the composition of metamaterials; their peculiar properties arise from their precise geometric structure and size scale. The microstructure and size scale is smaller than the wavelength it acts on, so they can influence the wave. They can be used in different applications, including stealth, waveguides, and electromagnetic wave adsorption [12–14]. Someone said that metamaterial physics plays the same role as those fields that have been issued Nobel prizes in physics [15]. Terahertz band refers to electromagnetic waves ranging from 0.1 to 10 THz bands in the middle of microwave and infrared bands [16–18]. Due to the weak interactions between molecules, [19–21]

✉ Zeng Qu
zqu@nuc.edu.cn

✉ Binzhen Zhang
zhangbinzhen@nuc.edu.cn

¹ Key Laboratory of Instrumentation Science & Dynamic Measurement, Ministry of Education, North University of China, Taiyuan 030051, China

² School of Electrical and Control Engineering, North University of China, Taiyuan 030051, China

³ School of Instrument and Electronics, North University of China, Taiyuan 030051, China

and some vibrations (e.g., skeletal vibrations of biological macromolecules, rotational and vibrational jumps of dipoles [22], and low-frequency vibrational absorption of lattices) are in the terahertz band [23], terahertz electromagnetic waves are very sensitive to detect small differences and changes in materials. Therefore, terahertz electromagnetic waves can be used in biomedical research to detect and identify biological macromolecules such as proteins, RNA, and DNA [24–26]. Furthermore, terahertz metamaterial bio-detection sensors based on microstructures [27, 28] can be used as a new detection tool to improve the sensor detection resolution and to achieve high quality [29, 30], rapid [31], and label-free detection [32], which has good development potential in bio-detection.

However, the terahertz metamaterial sensor still has some shortcomings: low Q value and low accuracy. Saadeddin et al. proposed a metamaterial terahertz sensor with a sensitivity of 300 GHz/RIU for chlorine detection in crops, but the Q value was only 22.05 [33]. In 2020, Ma et al. proposed a susceptible terahertz metamaterial sensor based on a center-symmetric double F-type metal structure [34]. With a sensitivity of up to 1800 GHz/RIU and a FOM of 15, this sensor can be used as a high-sensitivity biosensor. But its Q value is 49.6; a low Q value will affect the stability of the sensor. Wang et al. proposed a flexible metamaterial biosensor based on a flexible thin film (poly-phenylene-c, perylene-c) [35]. Simulation analysis showed that the sensitivity and FOM values were 243 GHz/RIU and 3.3 GHz, respectively, but the Q value was 14.2, affecting the sensor's accuracy. Similar results were found by Li et al. that the Q value was only 6.913 for the terahertz metamaterial biosensor used for the diagnosis of cirrhosis and hepatocellular carcinoma, and the accuracy and stability of the sensor were relatively poor [36]. The above research indicated that terahertz metamaterial biosensors have high sensitivity and

application prospects, but the small Q value makes the test accuracy low, significantly limiting its wide application.

Another disadvantage of the terahertz metamaterial sensor is that the sensitivity is insufficient for accurate detection. In 2020, Lin et al. proposed a terahertz metamaterial biosensor for detecting n carcinoembryonic antigen concentration, but its sensitivity was only 76.5 GHz/RIU [37]. A terahertz metamaterial biosensor is proposed for rapid and label-free identification of early cervical cancer tissue [38]. Although this method has the advantages of simplicity, label-free, and rapidity, its sensitivity is only 29 GHz/RIU, which significantly limits its wide application in the detection of tumor cells.

Given the above problems, a microstructure-based high- Q terahertz metamaterial bio-detection sensor is designed in this paper. When a terahertz wave is an incident on the sensor surface, it resonates with the microstructure and produces a narrow absorption peak. A detection channel is left in the middle of the sensor, and the absorption peak is shifted when the analyte is injected into the channel, and the concentration of the analyte, biomolecule content, etc., can be characterized by the magnitude of the shift. The working principle is shown in Fig. 1. The sensor can be integrated with a microfluidic cell screening chip or used alone. The sensor forms a resonant peak with an absorption of 98.9% of the resonance frequency of 0.4696 THz. The sensor has a sensitivity of up to 78.6 GHz/RIU, a Q of up to 55.3, and a FOM of up to 9.81. The quadruple rotation structure unit makes the sensor insensitive to wide incidence angles and polarization. The designed sensor features high sensitivity and high Q and FOM values, enabling the identification of biomolecules with different refractive indices, and has significant application prospects in medical diagnosis and real-time monitoring. It also provides new ideas for the design of terahertz band bio-detection sensors.

Fig. 1 Working principle of microstructure-based high- Q terahertz metamaterial bio-detection sensor

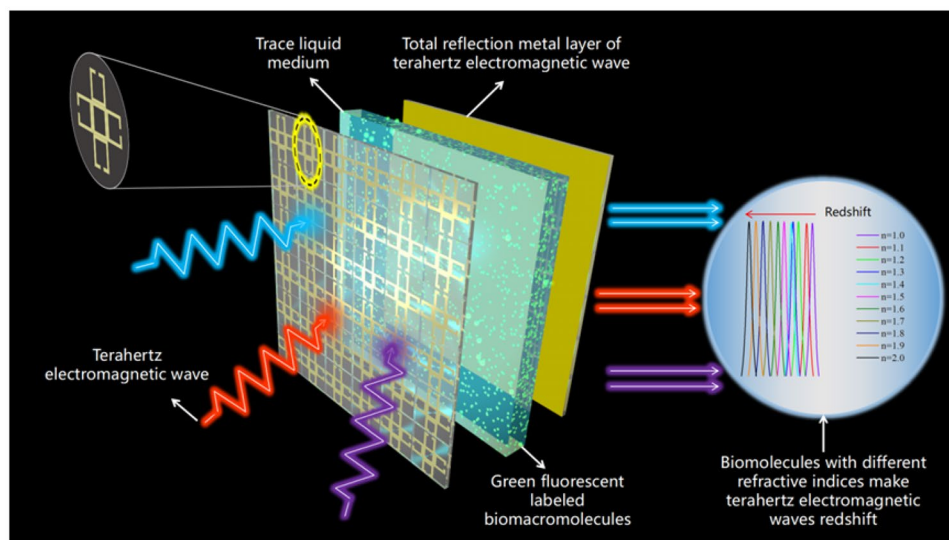
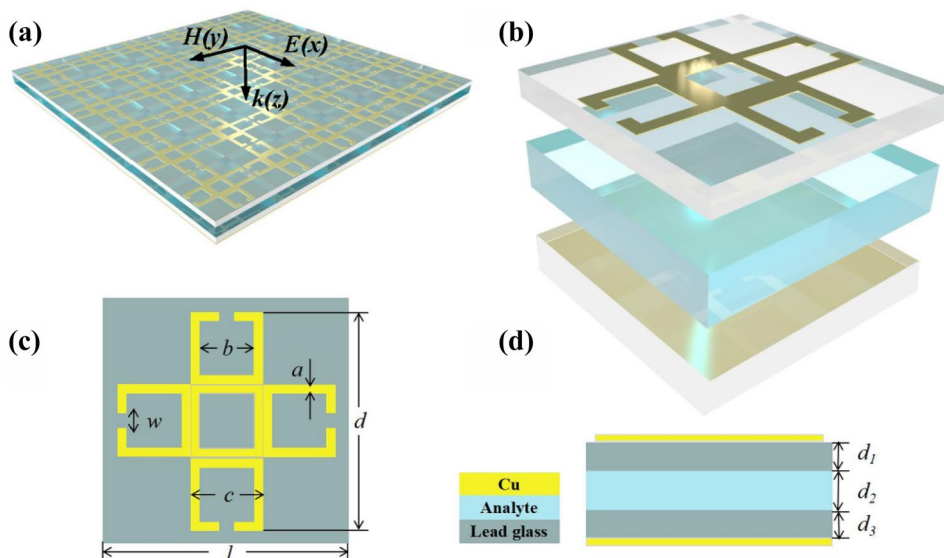


Fig. 2 Terahertz metamaterial bio-detection sensor with (a) periodic array, (b) cell structure, (c) frontal structure view, and (d) side view



2 Structural design and simulation

The designed sensor structure is depicted in Fig. 2. It consists of four functional layers: a metal microstructure layer, an analyte channel layer, a metal reflection layer, and a basal layer. Figure 2a presents a schematic diagram showing the periodic matrix arrangement of the sensor; Fig. 2b shows the unit structure of the sensor, where the metal microstructure consists of four identical metal open square rings and a nested metal square ring of the same size; Fig. 2c presents a front elevation of the sensor unit structure; and Fig. 2d shows a side elevation of the sensor unit structure. The detailed parameters of the metal microstructure of the sensor structure unit and the thickness of the unit structure are shown in Table 1. The absorption spectra were simulated and optimized using CST Microwave Studio 2020 based on the finite element method. In the simulation setting, the electric field E and magnetic field H are parallel to the incident plane, while the wave vector k is perpendicular to the incident plane. The structural elements were set as periodic boundaries along the x and y directions and the z direction as open space boundaries to establish the element model. The adaptive mesh was used to improve the structure’s simulation accuracy. The frequency domain solver was used to simulate the numerical value of the electromagnetic wave absorbed by the absorber. During the simulation, the metal microstructure and metal reflection layer used copper (Cu) material;

the conductivity is 5.8×10^7 S/m, and both thicknesses are $0.5 \mu\text{m}$. The channel layer of the analyte is between the metal microstructure layer and the metal reflection layer, the thickness d_2 is $30 \mu\text{m}$, and the refractive index range is set as $1 \sim 2$. The material used in the substrate is quartz glass (lead glass), and its dielectric constant and permeability are charged as 6 and 1.

3 Results and discussion

The absorption rate of the metamaterial absorber can be expressed by Eq. (1):

$$A(\omega) = 1 - R(\omega) - T(\omega) = 1 - |S_{11}|^2 - |S_{21}|^2 = 1 - |S_{11}|^2 \tag{1}$$

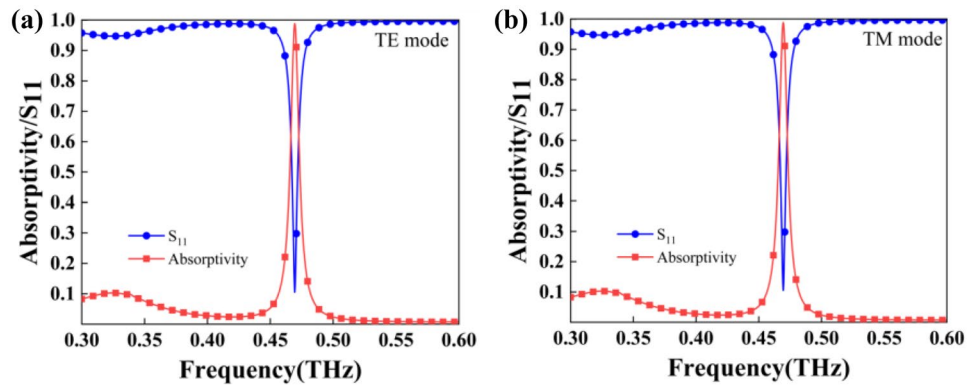
Among them, $R(\omega)$ and $T(\omega)$ denote the reflectance and transmittance of the metamaterial absorber, respectively, and S_{11} and S_{21} represent the reflectance and transmittance coefficients of the metamaterial absorber, respectively [39–41]. Since the reflective metal layer with a sensor thickness of $0.5 \mu\text{m}$ can effectively block the propagation of terahertz waves, the transmittance of the sensor to terahertz electromagnetic waves $T(\omega) = 0$.

Figure 3 shows the S_{11} and absorbance curves of the sensor in TE mode and TE mode with forwarding electromagnetic wave incidence. As can be seen from the graph, the sensor forms an absorption peak of up to 98.9% in the

Table 1 Detailed parameters of the microstructure and the thickness of the unit structure

Parameters	a	b	c	d	w	l	d_1	d_2	d_3
Value/ μm	12.5	40	65	195	5	200	100	30	100

Fig. 3 S_{11} and absorbance curves for (a) TE and (b) TM mode electromagnetic waves at the positive incidence.



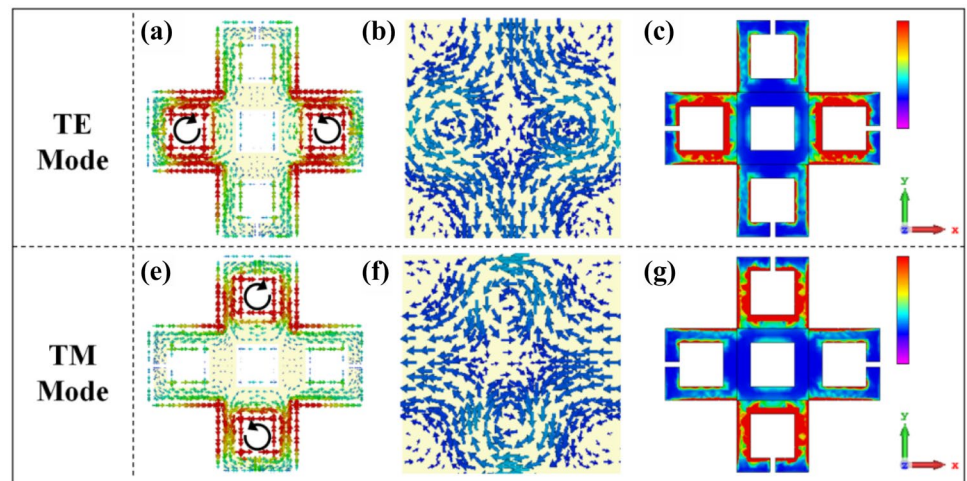
0.3–0.6 THz band, and the S_{11} and absorbance curves in both modes overlap perfectly.

3.1 Analysis of the absorption mechanism

The physical mechanism of the peak absorption of the sensor allows the analysis of the distribution of surface electric currents and energy losses at the resonant frequency point to be explored. From Fig. 3, the sensor forms 98.9% of the absorption peak over a resonant frequency of 0.4696 THz. The distribution of surface currents and energy loss in the X–Y plane of the sensor under the vertical incidence of terahertz electromagnetic waves in TE and TM modes is shown in Fig. 4. As can be seen in Fig. 4a and e, the four open square rings of the metal structure of the sensor produce induced currents in the TE mode for a resonant frequency of 0.4696 THz, with the left. Right open square rings produce induced currents in opposite directions, significantly more substantial than the top and bottom metal square rings. In TM mode, the induced currents generated by the upper and lower open square rings are in opposite directions, and the

intensity is significantly stronger than that of the two open square rings. As can be seen from Fig. 4b and f, in TE mode and TM mode, the direction of the induced current on the front of the metal structure is opposite to that on the metal back plate, and the two opposite surface currents form a loop. The direction of the magnetic field excited by this current ring coincides with that of the magnetic polarization of terahertz electromagnetic waves. The magnetic dipole effect between the two occurs, forming a magnetic resonance. When the induced current is generated on the sensor surface, it is known from the power loss equation $P_{loss} = I^2R$ (where P_{loss} shows the electromagnetic power loss, I is current at the surface, and R is the electrical resistance at the surface) that the induced current on the sensor surface will consume the electromagnetic wave in the form of thermal dissipation due to ohmic loss. From Fig. 4c and g, it can be seen that the electromagnetic wave loss in TE mode is mainly caused by the two open square rings on the right and left of the metal structural layer; the electromagnetic wave loss in TM mode is primarily caused by the two available square rings on the top and bottom of the metal structural layer.

Fig. 4 Plots of the front surface current of the metal structure, metal back surface current, and energy loss for (a)–(c) TE mode and (e)–(g) TM mode under the positive incidence of electromagnetic wave



To further analyze the absorption mechanism for the transducers, the equivalent impedance of the transducers was analyzed utilizing the impedance matching principle. When a terahertz electromagnetic wave is projected onto the sensory sensor, part of the incident electromagnetic wave is reflected off the sensor’s surface, and another part is transmitted through. It follows that to achieve maximum absorption, the reflection and transmission coefficients must be minimized. In general, sensors use a full metal backing plate of much greater thickness than the skin depth as their ground plane so that transmission is near zero. Thus, the absorptance of the sensor is determined mainly by the amount of reflectance [42–44].

The equivalent permittivity and equivalent permeability of the metamaterial absorber can be expressed as Eqs. (2) and (3):

$$\epsilon(\omega) = \epsilon' - j\epsilon'' \tag{2}$$

$$\mu(\omega) = \mu' - j\mu'' \tag{3}$$

Among them, ϵ' and μ' are the parameters describing the degree of polarization and magnetization, respectively, and ϵ'' and μ'' denote the electric and magnetic losses of the metamaterial absorber, respectively [45].

When the sensor’s resonant structural element dimensions are smaller than the wavelength at the corresponding operational frequency, the sensor as a whole can be considered an equivalent medium. Therefore, the equivalent impedance of the sensor can be derived from the equivalent capacitive weight $\mu(\omega)$ and the equivalent magnetic permeability $\epsilon(\omega)$ [46] can be expressed as Eq. (4):

$$Z(\omega) = \sqrt{\mu(\omega)/\epsilon(\omega)} \tag{4}$$

The relationship between the reflection coefficient S_{11} , transmission coefficient S_{21} [47], and the equivalent impedance of the sensor can be expressed as Eq. (5):

$$Z(\omega) = \sqrt{\frac{(1+S_{11})^2 - S_{21}^2}{(1-S_{11})^2 - S_{21}^2}} \tag{5}$$

When the electromagnetic wave is incident on the sensor surface, the degree of matching between its equivalent impedance and the free space impedance determines the magnitude of the reflection coefficient [46, 47], so the reflection coefficient $R(\omega)$ can be expressed as Eq. (6):

$$R(\omega) = |S_{11}|^2 = \left(\frac{Z(\omega) - 1}{Z(\omega) + 1}\right)^2 = \frac{[\text{Re}\{Z(\omega)\} - Z_0 \cos \theta]^2 + [\text{Im}\{Z(\omega)\}]^2}{[\text{Re}\{Z(\omega)\} + Z_0 \cos \theta]^2 + [\text{Im}\{Z(\omega)\}]^2} \tag{6}$$

where Z_0 is the wave impedance of the incident wave in free space, $Z_0 \approx 377 \Omega$, and θ is the angle of incidence of the electromagnetic wave. Thus, for a vertically incident electromagnetic wave with an incidence angle θ of 0, the reflectivity will be near zero as the normalized equivalent compound of the absorber impedance approaches 1 [48, 49].

The reflection coefficient $R(\omega)$ is obtained by rectifying the formula, as shown by Eq. (7):

$$R(\omega) = \frac{Z_L - Z_0}{Z_L + Z_0} \tag{7}$$

Among them, Z_L is the equivalent impedance of the sensor. When $Z_L = Z_0$ to meet the impedance matching, the reflection coefficient $R(\omega) = 0$ for the electromagnetic wave irradiated to the sensor in space. When the total impedance of a sensor is closer to the free-standing impedance of air, most of the electromagnetic energy is guaranteed to enter the sensor. The equivalent complex impedance frequency spectrum of the sensor is shown in Fig. 5. The equivalent complex impedance of the sensor at a resonant frequency of 0.4695 THz is $Z_L = 1.1 + i \times 0.018$, while the complex free-space impedance is $Z_0 = 1$. As a result, a good match of impedance is formed at the resonant frequency between the sensor on the one hand and the free space on the other, resulting in a high absorption resonance peak.

3.2 Incidence angle and polarization-sensitive characteristics analysis

In practical applications, sensors with wide incidence angles and polarization-insensitive characteristics can improve detection accuracy and reduce experimental

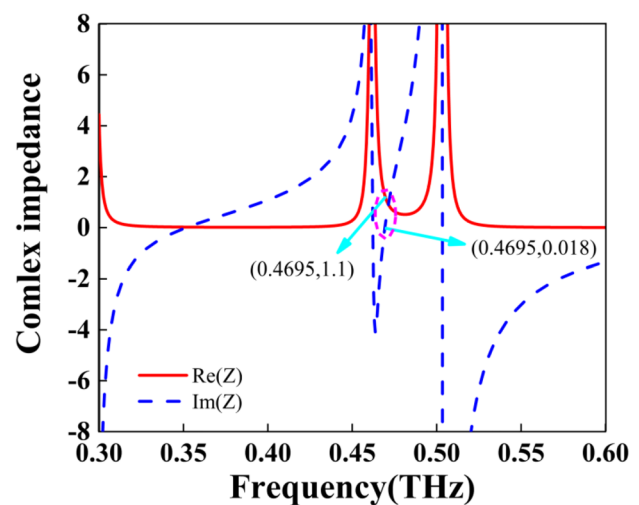
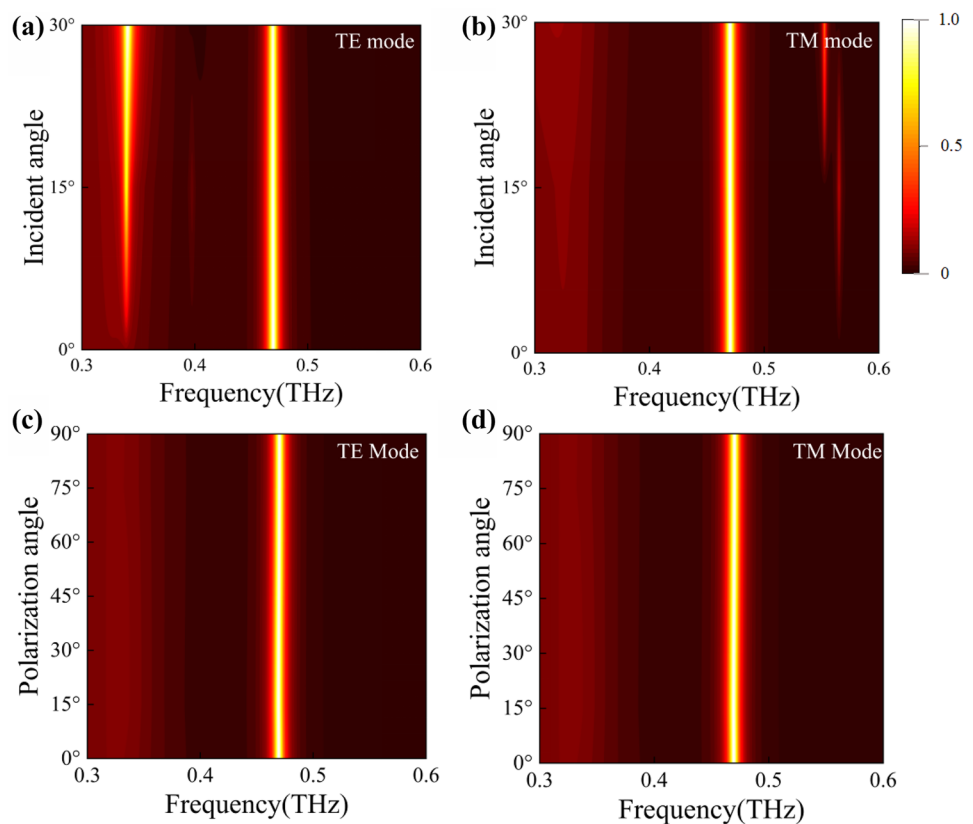


Fig. 5 Equivalent complex impedance frequency spectrum of the sensor

Fig. 6 Effect of variations of terahertz wave incidence angle and polarization angle on the absorbance of the sensor



errors, thus improving detection efficiency. Designing the sensing unit into a quadruple rotationally symmetric structure can realize the polarization-insensitive characteristics of the sensor. Figure 6a and b show the effect of the terahertz wave's incident angle variation on the sensor's absorption rate in the TM and TE modes, respectively. In TE mode, the absorbance of the sensor at the resonant frequency 0.4695 THz is higher than 96% for all the terahertz wave incident angles in the range of 0–30°, and no significant shift of the resonant frequency occurs. In the TM mode, the absorption rate at the resonant frequency 0.4695 THz was higher than 90% for both terahertz wave incident angles in the 0–30°, and no significant shift in the resonant frequency occurred. In addition, the sensor produced additional resonant peaks with increasing resonance rates as the angle of incidence of terahertz waves increased in TE and TM modes. This is because the resonance generated at the sensor surface increases with the increasing incident angle, resulting in additional resonance peaks. Since the other resonance peak is far from the resonance frequency of 0.4695 THz, it does not interfere with the sensor detection. The results mentioned above showed that the sensor maintains a high absorption rate when terahertz waves are incident at angles from 0 to 30° and have wide incidence angle insensitivity. Figure 6c and d show the effect of the polarization angle variation on the sensor's absorbance

in TE and TM modes. The absorbance and resonant frequency of the sensor remain unchanged under the vertical incidence of terahertz waves with a 0–90° polarization angle. So the sensor has good polarization insensitivity characteristics.

3.3 Sensing performance analysis

The sensor works by injecting analytes with different refractive indices into the sensor. At this point, the dielectric parameters of the sensor change, thus changing the resonance characteristics of the sensor (resonance frequency, absorbance, resonance peak, etc.). The analytes refer to cancer cells, proteins, nucleic acids, polysaccharide solutions, etc., ranging in size from a few nanometers to tens of nanometers, with refractive indices in the range of 1.0–2.0, enabling susceptible sensing detection in the terahertz frequency range.

Q , S , and FOM values represent the three indicators of sensor performance [50–52]. The Q value indicates a sensor's resonance characteristics, the size of which is relevant to both resolutions and sensitivity. In general, the higher the Q value, the smaller the dielectric loss of the structure and the narrower and sharper the resonance peak. The FOM value measures the sensor's overall

performance, and the higher the FOM value, the better the sensor’s performance. It is calculated by the following Eqs. (8), (9), and (10):

$$Q = \frac{f}{FWHM} \tag{8}$$

Here, f denotes the central resonant frequency, and FWHM (full-width half-height) denotes the half-peak width.

$$S = \frac{\Delta f}{\Delta n} \tag{9}$$

Here, Δn represents the amount of index of refraction change of the analyte, Δf represents the magnitude of the frequency shifts of the centroid frequency, and the sensitivity is in GHz/RIU (refractive index units).

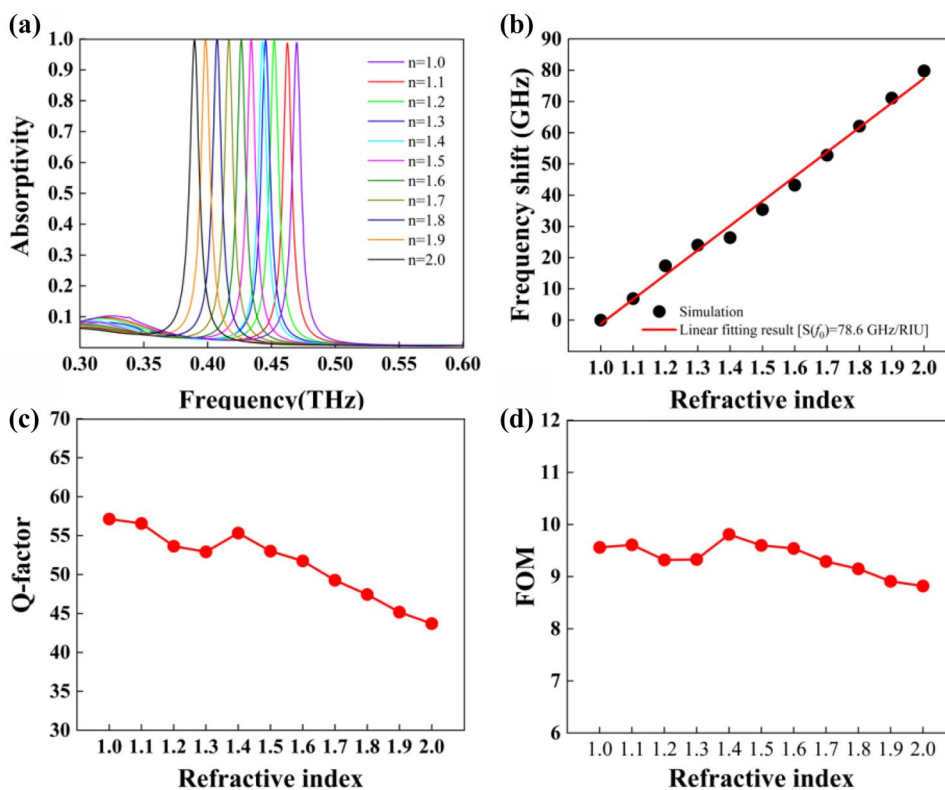
$$FOM = \frac{S}{FWHM} \tag{10}$$

The refractive indices of biomolecules usually range from 1.0 to 2.0, and for this purpose, the absorption characteristics of analytes are simulated when their refractive indices change. The simulation results in a redshift with increasing refractive power of the analytical material, and the resonance peak of the sensor is almost always above 99% absorption, as shown in Fig. 7a. Figure 7b shows the results of a linear fit to the resonant peak of the sensor

with a sensitivity of $S = 78.6$ GHz/RIU; Fig. 7c and d show the influence of the refractive index of the analyte upon the sensor’s Q and FOM values. It can be seen that as the refractive index increases, the Q of the resonant peak fluctuates slightly above and below 55. The FOM value fluctuates slightly above and below 9.6. When the refractive index of the analyte is 1.4, the Q value of the sensor is 55.32, and the maximum value of the FOM is 9.81. The excellent resonance characteristics indicate that the designed sensor has excellent performance and can achieve the identification of biomolecules with different refractive indices.

The terahertz sensor can shorten the detection time and improve the detection accuracy when detecting analytes in solution, enabling fast and accurate detection of liquid-phase analytes. The effect of the tangent to the analyte’s loss angle on the sensor’s absorbance when the real part of the analyte’s dielectric constant is 1 is shown in Fig. 8. It is seen that as the loss angle of the analyzed object increases tangentially, the resonant frequency of the sensor has a small redshift, and the absorbance and resonant intensity decrease simultaneously. The FWHM and Q values of the absorption peak also decrease with the increase of the loss angle tangent. Therefore, the sensor can distinguish the change in the loss angle of the object to be measured based on the change in absorbance and Q value.

Fig. 7 Influence of analytes with different refractive indices on the sensor sensing performance



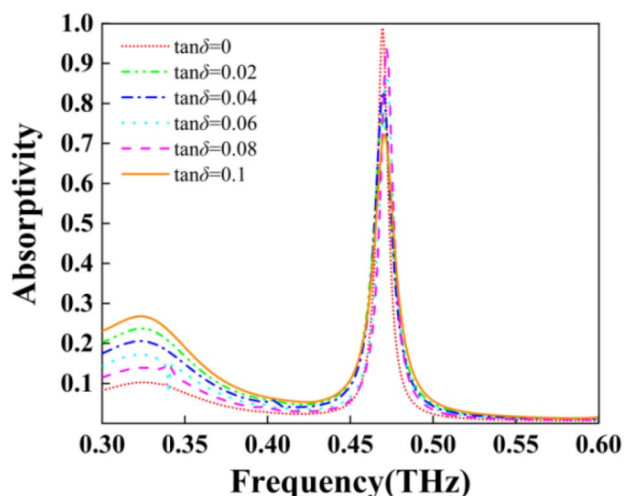


Fig. 8 Effect of analyte loss angle tangent on sensor absorbance

Table 2 compares the sensitivity, Q value, and FOM values of the proposed and terahertz sensors designed in the literature. It can be seen that the designed sensor has high Q and FOM values for analytes with different refractive indices, which indicates that the sensor has good accuracy and stability and has good prospects for applications in bio-detection and medical prevention.

4 Production process

After optimized design to confirm the optimal structural parameters, multiple cell samples were fabricated on 100- μm -thick lead glass substrate by lithography. Figure S1(a) and (b) show the fabrication flow chart. The process of making the metal structure layer is as follows: first will be treated as substrate after washing, then washed clean substrate with full positive photoresist, will be covered with the baseboard of photoresist after drying, use ultraviolet lithography at the positive photoresist substrate coated printing out

Table 2 Comparison of sensor sensitivity, Q value, and FOM value between the sensor proposed in this paper and those in the references

References	Operating band/THz	Sensitivity/ (GHz/RIU)	Quality factor	Figure of merit
29	1~2.2	300	22.05	2.94
30	5~6.5	1800	5.92	15
31	0.8~1.8	243	14.2	3.3
32	0.2~1	124	6.913	Not given
33	0.4~1.2	76.5	Not given	Not given
34	0.2~1	74	Not given	Not given
Proposed	0.3~0.6	78.6	55.3	9.81

the structure of the high-resolution image, adopt the method of lithography printing machine can implement high precision lithography in micro/nano level, thus greatly improve the accuracy of the finished product. After the lithography substrate is developed and examined to determine the correct structure of the lithography, the next step of sputtering can be carried out. The sputtering process requires using the magnetron sputtering method to sputter the pattern structure. The working principle is that the charged particles in the electromagnetic field will sputter to the substrate surface under the action of the electric field force. In this process, the charged particles collide violently with argon atoms, leading to the massive ionization of argon atoms, after the ionization of argon ions in the strong electric field under the action of high speed of cathode Cu target material surface caused by bombardment. The Cu atomic absorption of bombardment energy on the surface of the target material escapes from the surface of the target and deposition in the dielectric substrate, thus in the thickness of the dielectric substrate, to form a certain Cu membrane. This completes the surface Cu magnetron sputtering technology of the membrane. The structure designed in this paper is to sputter 20-nm and 135-nm-thick Ito-PET resistance films on the substrate, respectively. Finally, acetone and ethanol were used to ultrasonic clean the sample, and finally, the metal structure layer sample was obtained. The process of the metal reflection layer is as follows: after the substrate is cleaned and dried, the substrate is sputtered to obtain the metal reflection layer sample. The physical picture of the prepared sample and the microstructure under the electron microscope is shown in Figure S1(c)—(g).

5 Conclusion

To improve the accuracy and efficiency of the sensor in detecting and identifying biomolecules, we propose a high- Q terahertz metamaterial bio-detection sensor based on a combined square ring microstructure. It can break through the resolution limit of traditional biosensors to achieve highly sensitive, label-free, and rapid detection of biomolecules. The resonance characteristics of the sensor are changed by simulating the interaction of the bioanalyte with terahertz waves to achieve accurate and efficient identification. The results show that the sensor has a sensitivity of 78.6 GHz/RIU and maintains high Q and FOM values with high stability and sensitivity when the analyte refractive index ranges from 1.0 to 2.0 variations. In addition, the sensor has wide incidence angle insensitivity and polarization insensitivity characteristics. The designed microstructure-based terahertz metamaterial bio-detection sensor has high sensitivity and has a promising application in label-free, trace, fast, and efficient detection of analytes.

Supplementary Information The online version contains supplementary material available at <https://doi.org/10.1007/s42114-023-00679-4>.

Author contribution Zeng Qu and Jinfeng Kang prepared the main manuscript. Wei Li and Boyi Yao processed the data in Figs. 1, 2, and 3. Hao Deng and Yiqing Wei processed the data in Figs. 5, 6, 7, 8 and S1. Huihui Jing, Xiaohong Li, Junping Duan, and Binzhen Zhang did the chip process and proofreading, and all authors reviewed the manuscript.

Funding This work was supported by the National Natural Science Foundation of China (No. 52175555), the Top young and middle-aged innovative talents in Shanxi Colleges and universities, the Shanxi key research and development project (international cooperation) (No. 201803D421043), the fund for Shanxi “1331 Project” Key Subject Construction, the National Natural Science Foundation of China (innovation community) (No. 51821003), the Fundamental Research Program of Shanxi Province (No. 20210302123074), and the Fundamental Research Program of Shanxi Province (No.202203021212146).

Declarations

Competing interests The authors declare no competing interests.

Conflict of interest The authors declare no competing interests.

References

- Emaminejad H, Mir A, Farmani A (2021) Design and simulation of a novel tunable terahertz biosensor based on metamaterials for simultaneous monitoring of blood and urine components. *Plasmonics* 16(5):1537–1548. <https://doi.org/10.1007/s11468-021-01399-5>
- Wang Y, Wang Y, Hu F, Zeng L, Chen Z, Jiang M, Lin S, Guo W, Li D (2022) Surface-functionalized terahertz metamaterial biosensor used for the detection of exosomes in patients. *Langmuir* 38(12):3739–3747. <https://doi.org/10.1021/acs.langmuir.1c03286>
- Li Y, Chen X, Hu F, Li D, Teng H, Rong Q, Zhang W, Han J, Liang H (2019) Four resonators based high sensitive terahertz metamaterial biosensor used for measuring the concentration of protein. *J Phys D Appl Phys* 52(9):095105. <https://doi.org/10.1088/1361-6463/aaf7e9>
- Hou X, Chen X, Li T, Li Y, Tian Z, Wang M (2021) Highly sensitive terahertz metamaterial biosensor for bovine serum albumin (BSA) detection. *Optical Materials Express* 11(7):2268–2277. <https://doi.org/10.1364/ome.431339>
- Wang G, Zhu F, Lang T, Liu J, Hong Z, Qin J (2021) All-metal terahertz metamaterial biosensor for protein detection. *Nanoscale Res Lett* 16(1):109. <https://doi.org/10.1186/s11671-021-03566-3>
- Fang W, Lv X, Ma Z, Liu J, Pei W, Geng Z (2022) A flexible terahertz metamaterial biosensor for cancer cell growth and migration detection (Basel) 13(4):631. <https://doi.org/10.3390/mi13040631>
- Yang M, Zhang Z, Liang L, Yan X, Wei D, Song X, Zhang H, Lu Y, Wang M, Yao J (2019) Sensitive detection of the concentrations for normal epithelial cells based on Fano resonance metamaterial biosensors in the terahertz range. *Appl Opt* 58(23):6268–6273. <https://doi.org/10.1364/AO.58.006268>
- Cao L, Jia S, Thomson MD, Meng F, Roskos HG (2022) Can a terahertz metamaterial sensor be improved by ultra-strong coupling with a high-Q photonic resonator? *Opt Express* 30(8):13659–13672. <https://doi.org/10.1364/OE.456044>
- Azab MY, Hameed MFO, Nasr AM, Obayya SSA (2021) Highly sensitive metamaterial biosensor for cancer early detection. *IEEE Sens J* 21(6):7748–7755. <https://doi.org/10.1109/jsen.2021.3051075>
- Liu J, Fan L, Su J, Yang S, Luo H, Shen X, Ding F (2022) Study on a terahertz biosensor based on graphene-metamaterial. *Spectrochim Acta A Mol Biomol Spectrosc* 280:121527. <https://doi.org/10.1016/j.saa.2022.121527>
- Yang K, Li J, Lamy de la Chapelle M, Huang G, Wang Y, Zhang J, Xu D, Yao J, Yang X, Fu W (2021) A terahertz metamaterial biosensor for sensitive detection of microRNAs based on gold-nanoparticles and strand displacement amplification. *Biosens Bioelectron* 175:112874. <https://doi.org/10.1016/j.bios.2020.112874>
- Lin W, Huang S, Ren J (2020) Anomalous transient heat conduction in fractal metamaterials. *ES Energy Environ* 7:56–64. <https://doi.org/10.30919/eesee8c371>
- Guo J, Chen Z, El-Bahy ZM, Liu H, Abo-Dief HM, Abdul W, Abualnaja KM, Alanazi AK, Zhang P, Huang MN, Hu GM, Zhu JF (2022) Tunable negative dielectric properties of magnetic CoFe₂O₄/graphite-polyppyrole metacomposites. *Adv Compos Hybrid Mater* 5:899–906. <https://doi.org/10.1007/s42114-022-00485-4>
- Xie PT, Shi ZC, Feng M, Sun K, Liu Y, Yan KL, Liu CZ, Moussa TAA, Huang MN, Meng SW, Liang GM, Hou H, Fan RH, Guo ZH (2022) Recent advances in radio-frequency negative dielectric metamaterials by designing heterogeneous composites. *Adv Compos Hybrid Mater* 5:679–695. <https://doi.org/10.1007/s42114-022-00479-2>
- Huang JP (2019) Thermal metamaterials make it possible to control the flow of heat at will-2. *ES Energy Environ* 6:1–3. <https://doi.org/10.30919/eesee8c379>
- Tang M, Xia L, Wei D, Yan S, Zhang M, Yang Z, Wang H, Du C, Cui H L (2020) Rapid and label-free metamaterial-based biosensor for fatty acid detection with terahertz time-domain spectroscopy. *Spectrochim Acta A Mol Biomol Spectrosc* 228:117736. <https://doi.org/10.1016/j.saa.2019.117736>
- Liu J (2020) High-sensitivity detection method for organochlorine pesticide residues based on loop-shaped absorber. *Mater Chem Phys* 242:122542. <https://doi.org/10.1016/j.matchemphys.2019.122542>
- Deng X, Shen Y, Liu B, Song Z, He X, Zhang Q, Ling D, Liu D, Wei D (2022) Terahertz metamaterial sensor for sensitive detection of citrate salt solutions. *Biosensors (Basel)* 12(6):408. <https://doi.org/10.3390/bios12060408>
- Keshavarz A, Vafapour Z (2019) Sensing avian influenza viruses using terahertz metamaterial reflector. *IEEE Sens J* 19(13):5161–5166. <https://doi.org/10.1109/jsen.2019.2903731>
- Li D, Lin S, Hu F, Chen Z, Zhang W, Han J (2020) Metamaterial terahertz sensor for measuring thermal-induced denaturation temperature of insulin. *IEEE Sens J* 20(4):1821–1828. <https://doi.org/10.1109/jsen.2019.2949617>
- Tang C, Yang J, Wang Y, Cheng J, Li X, Chang C, Hu J, Lü J (2021) Integrating terahertz metamaterial and water nanodroplets for ultrasensitive detection of amyloid β aggregates in liquids. *Sens Actuators B Chem* 329:129113. <https://doi.org/10.1016/j.snb.2020.129113>
- Zhang J, Mu N, Liu L, Xie J, Feng H, Yao J, Chen T, Zhu W (2021) Highly sensitive detection of malignant glioma cells using metamaterial-inspired THz biosensor based on electromagnetically induced transparency. *Biosens Bioelectron* 185:113241. <https://doi.org/10.1016/j.bios.2021.113241>
- Cao P, Wu Y, Wang Z, Li Y, Zhang J, Liu Q, Cheng L, Niu T (2020) Tunable dual-band ultrasensitive stereo metamaterial terahertz sensor. *IEEE Access* 8:219525–219533. <https://doi.org/10.1109/access.2020.3039503>
- Veeraselvam A, Mohammed GNA, Savarimuthu K (2021) A novel ultra-miniaturized highly sensitive refractive index-based terahertz biosensor. *J Lightwave Technol* 39(22):7281–7287. <https://doi.org/10.1109/jlt.2021.3112529>
- Xu W, Xie L, Zhu J, Tang L, Singh R, Wang C, Ma Y, Chen H-T, Ying Y (2019) Terahertz biosensing with a graphene-metamaterial

- heterostructure platform. *Carbon* 141:247–252. <https://doi.org/10.1016/j.carbon.2018.09.050>
26. Zhang R, Chen Q, Liu K, Chen Z, Li K, Zhang X, Xu J, Pickwell-MacPherson E (2019) Terahertz microfluidic metamaterial biosensor for sensitive detection of small-volume liquid samples. *IEEE Transactions on Terahertz Science and Technology* 9(2):209–214. <https://doi.org/10.1109/tthz.2019.2898390>
 27. Liang W, Zuo J, Zhou Q, Zhang C (2022) Quantitative determination of glycerol concentration in aqueous glycerol solutions by metamaterial-based terahertz spectroscopy. *Spectrochim Acta A Mol Biomol Spectrosc* 270:120812. <https://doi.org/10.1016/j.saa.2021.120812>
 28. Liu K, Zhang R, Liu Y, Chen X, Li K, Pickwell-Macpherson E (2021) Gold nanoparticle enhanced detection of EGFR with a terahertz metamaterial biosensor. *Biomed Opt Express* 12(3):1559–1567. <https://doi.org/10.1364/BOE.418859>
 29. Niu Q, Zhang R, Yang Y (2022) High sensitivity and label-free detection of the SARS-CoV-2 S1 protein using a terahertz meta-biosensor. *Front Phys* 10:859924. <https://doi.org/10.3389/fphy.2022.859924>
 30. Keshavarz A, Vafapour Z (2019) Water-based terahertz metamaterial for skin cancer detection application. *IEEE Sens J* 19(4):1519–1524. <https://doi.org/10.1109/jsen.2018.2882363>
 31. Fang W, Ma Z, Lv X, Liu J, Pei W, Geng Z (2022) Flexible terahertz metamaterial biosensor for label-free sensing of serum tumor marker modified on a non-metal area. *Opt Express* 30(10):16630–16643. <https://doi.org/10.1364/oe.454647>
 32. Zhou J, Zhao X, Huang G, Yang X, Zhang Y, Zhan X, Tian H, Xiong Y, Wang Y, Fu W (2021) Molecule-specific terahertz biosensors based on an aptamer hydrogel-functionalized metamaterial for sensitive assays in aqueous environments. *ACS Sens* 6(5):1884–1890. <https://doi.org/10.1021/acssensors.1c00174>
 33. Saadeldin AS, Hameed MFO, Elkaramany EMA, Obayya SSA (2019) Highly sensitive terahertz metamaterial sensor. *IEEE Sens J* 19(18):7993–7999. <https://doi.org/10.1109/jsen.2019.2918214>
 34. Ma A, Zhong R, Wu Z, Wang Y, Yang L, Liang Z, Fang Z, Liu S (2020) Ultrasensitive THz sensor based on centrosymmetric F-shaped metamaterial resonators. *Front Phys* 8:584639. <https://doi.org/10.3389/fphy.2020.584639>
 35. Wang Z, Geng Z, Fang W (2020) Exploring performance of THz metamaterial biosensor based on flexible thin-film. *Opt Express* 28(18):26370–26384. <https://doi.org/10.1364/OE.402222>
 36. Li D, Zeng L, Wang Y, Tang H-W, Lee WX, Chen Z, Zhang L, Zou Y, Xie D, Hu F (2022) Terahertz metamaterial biosensor for diagnosis of hepatocellular carcinoma at early stage. *Appl Opt* 61(16):4817–4822. <https://doi.org/10.1364/ao.459489>
 37. Lin S, Xu X, Hu F, Chen Z, Wang Y, Zhang L, Peng Z, Li D, Zeng L, Chen Y, Wang Z (2021) Using antibody modified terahertz metamaterial biosensor to detect concentration of carcinoembryonic antigen. *IEEE J Sel Top Quantum Electron* 27(4):1–7. <https://doi.org/10.1109/jstqe.2020.3038308>
 38. Li D, Hu F, Zhang H, Chen Z, Huang G, Tang F, Lin S, Zou Y, Zhou Y (2021) Identification of early-stage cervical cancer tissue using metamaterial terahertz biosensor with two resonant absorption frequencies. *IEEE J Sel Top Quantum Electron* 27(4):1–7. <https://doi.org/10.1109/jstqe.2021.3058163>
 39. Jing H, Duan J, Wei Y, Hao J, Qu Z, Wang J, Zhang, B (2022) An ultra-broadband flexible polarization-insensitive microwave metamaterial absorber. *Mater Res Express* 9:025802. <https://doi.org/10.1088/2053-1591/ac5484>
 40. Cheng H, Lu Z, Gao Q, Zuo Y, Liu X, Guo Z, Liu C, Shen C (2021) PVDF-Ni/PE-CNTs composite foams with co-continuous structure for electromagnetic interference shielding and photo-electro-thermal properties. *Eng Sci* 16:331–340. <https://doi.org/10.30919/es8d518>
 41. Wu N, Du W, Hu Q, Vupputuri S, Jiang Q (2021) Recent development in fabrication of co nanostructures and their carbon nanocomposites for electromagnetic wave absorption. *Eng Sci* 13:11–23. <https://doi.org/10.30919/es8d1149>
 42. Smith DR, Vier DC, Koschny T, Soukoulis CM (2005) Electromagnetic parameter retrieval from inhomogeneous metamaterials. *Phys Rev E* 71(3 Pt.2):036617. <https://doi.org/10.1103/PhysRevE.71.036617>
 43. Wang H, Sivan VP, Mitchell A, Rosengarten G, Phelan P, Wang LP (2015) Highly efficient selective metamaterial absorber for high-temperature solar thermal energy harvesting. *Sol Energy Mater Sol Cells* 137:235–242. <https://doi.org/10.1016/j.solmat.2015.02.019>
 44. Guo Y, Liu H, Wang DD, El-Bahy ZM, Althakafy JT, Abo-Dief HM, Guo ZH, Xu BB, Liu CT, Shen CY (2022) Engineering hierarchical heterostructure material based on metal-organic frameworks and cotton fiber for high-efficient microwave absorber. *Nano Res* 15(8):6841–6850. <https://doi.org/10.1007/s12274-022-4533-x>
 45. Liu R, Cui TJ, Huang D, Zhao B, Smith DR (2007) Description and explanation of electromagnetic behaviors in artificial metamaterials based on effective medium theory. *Phys Rev E* 76(2 Pt 2):026606. <https://doi.org/10.1103/PhysRevE.76.026606>
 46. Wang G, Wu T, Jia Y, Gao Y, Gao Y-C (2022) Switchable terahertz absorber from single broadband to triple-narrowband. *Diam Relat Mater* 130:0925–9635. <https://doi.org/10.1016/j.diamond.2022.109460>
 47. Jing H-H, Wei Y-Q, Kang J-F, Song C-W, Deng H, Duan J-P, Qu Z, Wang J-Y, Zhang B-Z (2023) An optically transparent flexible metasurface absorber with broadband radar absorption and low infrared emissivity. *J Phys D Appl Phys* 56(11):115103. <https://doi.org/10.1088/1361-6463/acbbda>
 48. Guo J, Chen Z, Xu X, Li X, Liu H, Xi S, Abdul W, Wu Q, Zhang P, Xu B, Zhu J, Guo Z (2022) Enhanced electromagnetic wave absorption of engineered epoxy nanocomposites with the assistance of polyaniline fillers. *Advanced Composites and Hybrid Materials* 5(3):1769–1777. <https://doi.org/10.1007/s42114-022-00417-2>
 49. Guo J, Li X, Chen Z, Zhu J, Mai X, Wei R, Sun K, Liu H, Chen Y, Naik N, Guo Z (2022) Magnetic NiFe₂O₄/Polypyrrole nanocomposites with enhanced electromagnetic wave absorption. *J Mater Sci Technol* 108:64–72. <https://doi.org/10.1016/j.jmst.2021.08.049>
 50. Yue L, Wang Y, Cui Z, Zhang X, Zhu Y, Zhang X, Chen S, Wang X, Zhang K (2021) Multi-band terahertz resonant absorption based on an all-dielectric grating metasurface for chlorpyrifos sensing. *Opt Express* 29(9):13563–13575. <https://doi.org/10.1364/OE.423256>
 51. Wang Y, Zhu D, Cui Z, Yue L, Zhang X, Hou L, Zhang K, Hu H (2020) Properties and sensing performance of all-dielectric metasurface THz absorbers. *IEEE Trans Terahertz Sci Technol* 10(6):599–605. <https://doi.org/10.1109/TTHZ.2020.3010164>
 52. Qi Y, Zhang Y, Liu C, Zhang T, Zhang B, Wang L, Deng X, Bai Y, Wang X (2020) A tunable terahertz metamaterial absorber composed of elliptical ring graphene arrays with refractive index sensing application. *Results Phys* 16:103012. <https://doi.org/10.1016/j.rinp.2020.103012>

Publisher's Note Springer Nature remains neutral with regard to jurisdictional claims in published maps and institutional affiliations.

Springer Nature or its licensor (e.g. a society or other partner) holds exclusive rights to this article under a publishing agreement with the author(s) or other rightsholder(s); author self-archiving of the accepted manuscript version of this article is solely governed by the terms of such publishing agreement and applicable law.